Characterization of oxygen vacancies in SrTiO 3 by means of anelastic and Raman spectroscopy

D. Chapron, Francesco Cordero, Marc Fontana

Characterization of oxygen vacancies in $SrTiO_3$ by means of anelastic and Raman spectroscopy

David Chapron,[1] Francesco Cordero,[2] and Marc D. Fontana[1]
[1)] *Université de Lorraine, Laboratoire Matériaux Optiques, Photonique et Systèmes, EA 4423, 2 rue Edouard Belin, 57070 Metz, France.*
CentraleSupélec, Laboratoire Matériaux Optiques, Photonique et Systèmes, EA 4423, 2 rue Edouard Belin, 57070 Metz, France.[a)]
[2)] *CNR, Istituto di Struttura della Materia (ISM-CNR) Area della Ricerca di Roma-Tor Vergata, Via del Fosso del Cavaliere, 100,I-00133 Roma, Italy*

(Dated: 20 August 2019)

Oxygen vacancies in reduced $SrTiO_3$ are investigated by Raman spectroscopy and dynamic elastic modulus measurements. The anelastic spectrum is used to evaluate the amount and state of the O vacancies, which result to be almost completely paired and otherwies aggregated at a concentration of 0.5 mol%, with only 1/6 of them isolated at room temperature. Raman spectra recorded as a function of temperature in as-grown and reduced samples are examined regarding the different processes which can contribute to them. Chemometric analysis is used to highlight the specific influence of oxygen vacancies on the Raman spectra. It is shown that oxygen vacancies induce a relaxation of selection rules leading to the activation of first-order lines even in the cubic phase. Furthermore, regions around oxygen vacancies are demonstrated to be responsible for the asymmetric broadening of Raman line.

Keywords: strontium titanate, oxygen vacancies, Raman spectroscopy, PCA

I. INTRODUCTION

Among the ABO_3 perovskite compounds $SrTiO_3$ (STO) shows peculiar interest for fundamental research and applications as well. On the one hand it is generally considered as a textbook example of quantum paraelectric, since it remains paraelectric down to 0 K[1]. On the other hand, due to the high dielectric permittivity, it is an attractive material for microwave or THz devices, and dynamic random access memories[2]. Point defects play an important role, in particular for electrical and electrochemical applications. Oxygen vacancies (V_O) govern the transport properties and can induce a superconducting state, which is still under study[3]. In addition, they may induce a state of giant permittivity, interesting for capacitors and energy storage devices[4] and participate in filamentary resistive switching[5]. Furthermore, V_O are considered to be responsible for electrical breakdown and damage in microelectronic devices.

Notwithstanding the importance of V_O in determining the electrical properties of STO, and their use for this purpose, the literature is confusing regarding their mobility, and very little is actually known on their aggregation state. There is a large spread of data for the diffusivity of V_O in STO, but they are usually considered as uniformly dispersed and diffusing with an activation energy of about 1 eV. The only techniques that can probe the hopping of isolated V_O in perovskites are anelastic[6] and NMR[7] relaxation, and agree on a barrier of 0.6 eV both for isolated V_O free in the lattice[6] and trapped by acceptor Fe[7]. This is a much faster mobility than generally found, but the anelastic experiments also show that most V_O aggregate in pairs and larger clusters already at concentrations as low as 0.5 mol% below 800 K; the activation energy for the motion of the aggregated V_O is 1 eV[6], explaining why this is the value generally found. While the more extended clusters of V_O have been assumed to be chains for the purpose of fitting the anelastic spectra, their nature is actually unknown. Yet, the nature of the aggregations of the V_O is certainly of great interest in connection with the relatively stable confinement in near surface regions[8] or filamentary defects responsible for resistive switching[5].

Raman spectroscopy is known to be an efficient tool for studying vibrational modes and structural phase transitions. It can also provide information on point defects introduced in the lattice, by studying the change of the spectra[9]. Therefore, the question of the ability of Raman spectroscopy to probe oxygen vacancies is of primary interest.

Ten years ago, Tenne et al. have investigated the effect of reduction on the Raman spectra (RS) of STO[10]. They found two effects: the appearance of first order peaks corresponding to optical phonons of the STO lattice and new lines attributed to local vibrational modes related to the oxygen vacancies. Nevertheless, this interpretation is debatable owing to the complexity of the RS and the various processes which can contribute to them. Thus the RS in cubic STO includes the possible coexistence of strong and broad second order scattering and first order peaks of different origins[11–13]. The first-order RS is in principle forbidden in a centrosymmetric phase, so that only second-order scattering should be detected. In fact first-order peaks can be observed in the cubic phase due to the disappearance of inversion symmetry, which can be caused by a deviation from stoichiometry[14], the

[a)] Electronic mail: david.chapron@univ-lorraine.fr

presence of impurities or dopant ions[15], the grains[16] or to the existence of strains, particularly in thin films[17]. Furthermore, some additional lines appear below the antiferrodistortive (AFD) transition at 105 K, and are due to unit cell doubling and attributed to phonons at the Brillouin zone boundary point R[13]. All these peaks show their own dependence on temperature (T). This renders difficult the analysis of the effect of the different processes.

Therefore, we have undertaken a new Raman investigation of V_O in STO with the comparison of the spectra in as-grown and reduced single crystals, by means of principal components analysis (PCA), which is able to evidence the variability (even very small) between spectra (or data) due to any external parameter change. The reduced sample was firstly studied by means of anelastic measurements in order to reliably characterize the concentration and state of the oxygen vacancies.

The samples were cut from a wafer of STO 0.5 mm thick from M.T.I. Corporation. One sample was left in the virgin transparent state, while the other, was cut as a bar approximately 28 x 2.6 x 0.5 mm^3, with the edges parallel to the (100) directions, for the anelastic measurement. In order to reduce it, it was inserted in an envelope of Pt foil open at both ends, sitting inside a water cooled quartz tube and heated by induction, as described in[6]. The sample was heated to approximately 1150 °C for 3 h in a flux of 0.9Ar + 0.1CO maintained at 920 mbar, followed by 1 h homogenization at 800 °C in the same flux. The O deficiency deduced from the mass loss was $\delta = 0.0043$ in $SrTiO_{3-\delta}$, but there is some uncertainty on an estimate only based on the mass loss; for example, it is impossible to assess if the sample picked up some material from the heated Pt foil. In order to have a better characterization of the concentration and state of the O vacancies, the complex dynamic Young's modulus $E = E' + iE''$ of the reduced sample was measured between 90 and 650 K. The sample was suspended on thin thermocouple wires in correspondence to the nodal lines of the first flexural resonance (5.0 kHz) and electrostatically excited in high vacuum or <0.1 mbar He, as described in ref[18]. The Young's modulus is obtained from the resonance frequency, $E' \propto f^2$, and the elastic energy loss, $Q^{-1} = E''/E'$, from the decay of the free oscillations, after switching off the excitation. The measurements were made during both heating and cooling.

II. RESULTS

1. Anelastic spectra

Figure 1 shows the real part E' of the Young's modulus, $E = 1/s_{11}$ normalized to its maximum value, and the elastic energy loss Q^{-1} of the reduced sample measured at 5 and 27 kHz during the same cooling and heating runs. The third flexural mode at higher frequency could be measured reliably only in limited temperature intervals, but enough to see the temperature dependence of the intensity of peak P3.

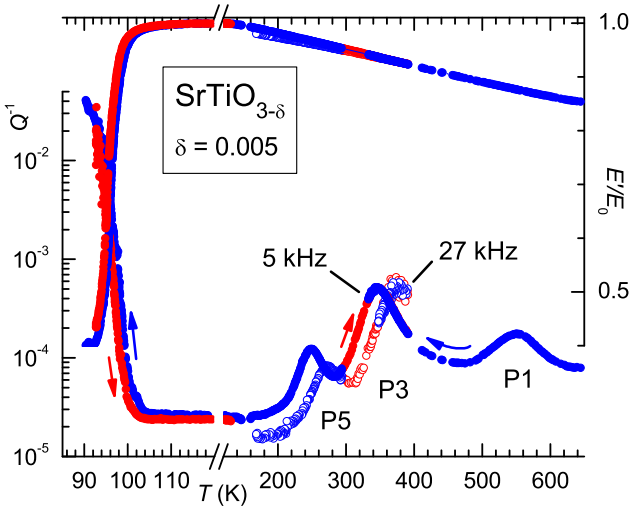

FIG. 1. Elastic energy loss and normalized Young's modulus of the reduced sample. The arrows indicate cooling and heating.

In the present context we are interested in the $Q^{-1}(T)$ curves, which contain peaks associated with various anelastic relaxation processes from hopping of V_O and rearrangements of their complexes under the influence of the applied stress at frequency $\omega/2\pi$. Consider the case of an isolated V_O hopping with characteristic time $\tau = \tau_0 \exp(W/kT)$. Each jump is accompanied by a reorientation of 90 ° of the direction of the nearest neighbour Ti atoms, and hence of the associated local distortion, or elastic dipole tensor λ. The populations of the three possible types of sites for the V_O with Ti along x, y and z, otherwise identical, are perturbed by the external stress and the resulting anelastic relaxation produces a Debye peak in the losses[6]:

$$Q^{-1}(T) \propto \frac{c(\Delta\lambda)^2}{T} \frac{\omega\tau}{1+(\omega\tau)^2}, \qquad (1)$$

where c is the (temperature dependent) volume concentration of the isolated V_O, $\Delta\lambda$ the change of the elastic dipole after a jump, projected in the direction of the applied stress, and τ is the defect hopping time, apart from a factor close to unity. The maximum is at the temperature T_m such that $\omega\tau(T_m) \cong 1$, so that the same process measured at higher frequency is shifted to higher temperature. Jumps of isolated V_O, reorientations of pairs and aggregation/dissolution of complexes occur with different characteristic times and produce different peaks in the anelastic spectrum $Q^{-1}(\omega, T)$.

The virgin sample has a flat $Q^{-1}(T)$ curve above 110 K, with none of the peaks found in the reduced samples, and labeled according to[6] (see curve 1 in Fig. 2). The peaks certainly associated with the hopping of V_O

are P1 and P3. P3 is due to the jumps of isolated V_O, while P1 to the reorientation of pairs, but the formation of larger and more stable aggregates of V_O, possibly longer chains, has been deduced from the dependence of the intensity of P1 on temperature and annealing[6]. Peak P5 is probably due to small polarons introduced by the V_O. The sharp rise of dissipation and drop of modulus below 100 K (Fig. 1) is due to the AFD transition. Its shift to lower temperature with respect to the undoped case (105 K) allows the O deficiency to be assessed independently of the mass loss[6], but a full comparison of the anelastic spectrum with those measured under various level of reduction from Ref.[6] (Fig. 2) is useful to discuss the state, in addition to the concentration of the V_O in the presently reduced sample.

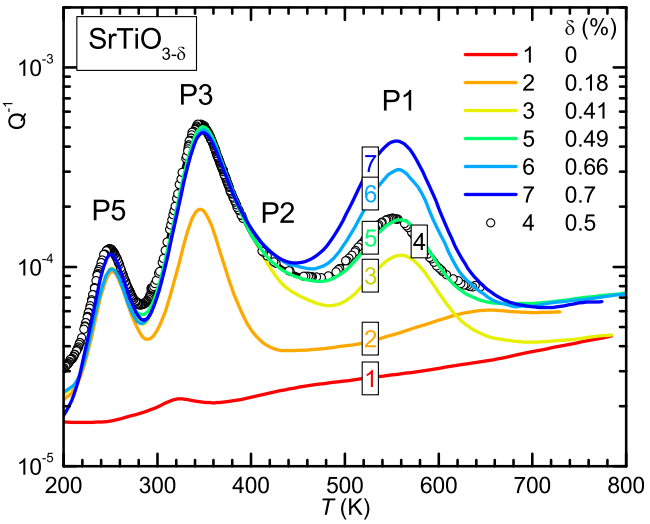

FIG. 2. Anelastic spectrum of the reduced sample (curve 4), plotted together with other spectra at various O deficiencies δ taken from Ref.[6].

The continuous lines in Fig. 2 and the present data (empty symbols) are close to the curve of $\delta = 0.0049$. According to this comparison, the present δ is slightly greater than 0.0049, but certainly smaller than 0.0066, so that we may estimate the O deficiency as $\delta = 0.0050 \pm 0.0005$, not far from the estimate from the mass loss.

Figure 3 shows the calculated fractions of V_O that are free, paired and aggregated (including paired), assuming $\delta = 0.005$ and the approximations and parameters described in detail in Ref.[6] for fitting the $Q^{-1}(T)$ curves. The approximation consists in dividing the crystal into non overlapping regions, for each of which a grand partition function can be constructed[19] including V_O that are free or aggregated into pairs or chains of length up to four. The following parameters have been used, setting the energy of an isolated V_O as $E_f = 0$: E_p/k_B = -2140 K for paired V_O and E_c/k_B = -3000 K for V_O inside chains of 3 to 4 vacancies, the V_O at the ends being considered as paired. From Fig. 3 it appears that at room temperature the majority of V_O is aggregated and less than 1/6 of

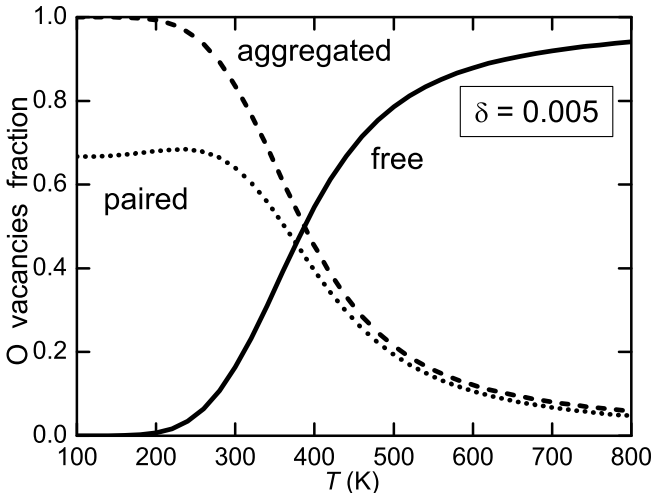

FIG. 3. Fractions of free, paired and total aggregated fraction of the V_O, assuming $\delta = 0.005$ and the approximations and parameters of Ref.[6].

them are isolated; the fraction is further reduced at lower temperature. That the crossover region between aggregated and free V_O is slightly above room temperature can be qualitatively checked by observing the temperature dependence of the intensity of P3, due to free V_O. The intensities of the Debye relaxation peaks of defects with constant concentrations decrease as $1/T$, but P3 increases instead with T (compare the curves measured at different frequencies in Fig. 1), due to the thermal dissolution from the aggregated to the free state, which increases the fraction of free V_O[6].

The Raman data described below are aimed at providing: (i) spectral signatures of V_O by comparing measurements on as-grown and reduced samples (ii) possibly information on the aggregation state of V_O.

2. Raman spectra

Raman measurements were carried out by means of Aramis Horiba Jobin-Yvon spectrometer with a 532 nm laser at a power of 50 mW as the exciting line. The resolution was 1.2 cm^{-1}. Measurements were performed as function of temperature from room T down to 93 K, i.e. just below the phase transition temperature (105 K) by placing the sample on a Linkam THMS600 stage.

Figure 4 shows the Raman spectrum recorded for different temperatures in the untreated crystal. At room temperature the spectrum exhibits several broad bands labelled 1 to 9, well attributed to 2^{nd} order scattering[11–13], which is solely expected by Raman selection rules for the stoichiometric crystal in the cubic phase. At 93 K, i.e. below the AFD transition, two new lines denoted R and lying at 143 and 449 cm^{-1} occur in the tetragonal phase. They are due to a folding of the

Brillouin zone (BZ) resulting from cell doubling, so that the phonon modes at the zone boundary point R appear at the BZ center in the tetragonal phase and are therefore detected by Raman spectroscopy. The phonons R are associated with antiphase tilting of the Ti-O_6 octahedra.

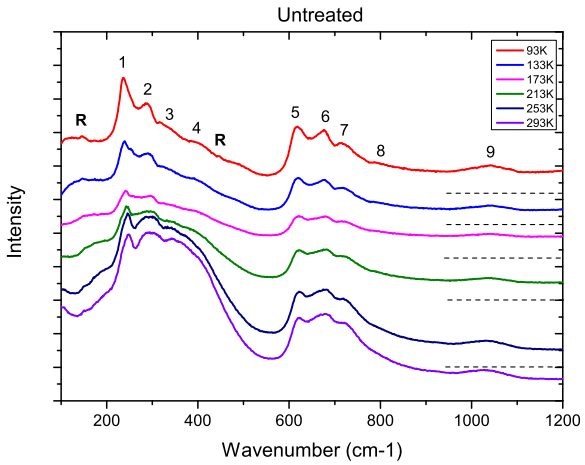

FIG. 4. Raman spectra of the untreated sample as function of T. The second order bands are labelled 1 to 9. R denote the lines linked to the AFD transition.

It is to be noted that no additional lines, that could be assigned to impurities, are detected, proving the stoichiometric and undoped nature of the crystal under study. Therefore, the comparison with spectra on reduced sample, prepared from the same crystal, should be more reliable, since any difference between them can be related to the treatment only.

The spectra of the reduced sample, shown in figure 5, displays the second-order bands and R peaks located at the same positions as in the untreated sample, but new lines labelled A, B and C are detected around 175, 549, and 860 cm^{-1}. On cooling, these peaks become narrower and increase in intensity so that they more and more emerge from broad 2^{nd} order scattering.

No significant shift of the positions of the lines A, B and C is detected with change of T. It is to be noted that the peaks A and B are asymmetric. In addition to the appearance of new lines A, B and C, the spectra in the reduced sample differ from that in the untreated sample by the occurrence of a broad signal below 150 cm^{-1}. Its origin is not clear, since we did not perform measurements at lower frequency owing to the use of edge filter for suppressing the Rayleigh line.

In figure 6 are compared the spectra recorded at the same T (93 K) in both crystals, pointing out the new lines A, B and C in the reduced crystal. These bands can be straightforwardly related to the presence of oxygen vacancies in this crystal. This feature is corroborated below by PCA.

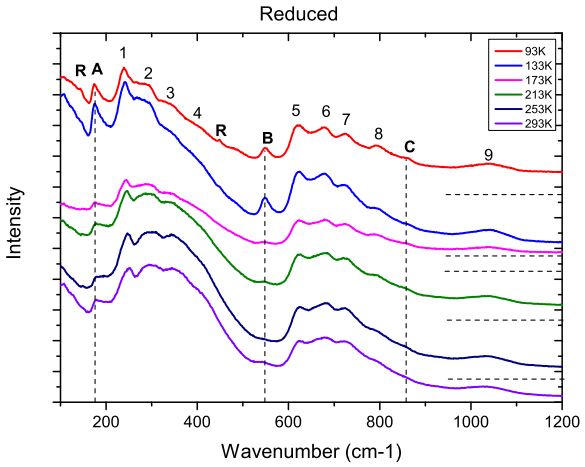

FIG. 5. Raman spectra of the reduced sample as function of T. The second order bands are labelled 1 to 9. R denote the lines linked to the AFD transition.

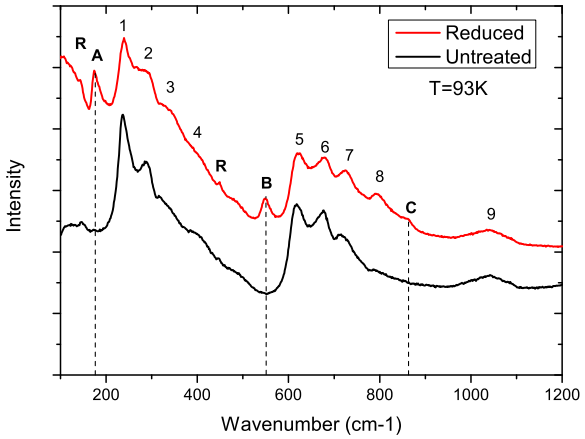

FIG. 6. Comparison of Raman spectra between untreated and reduced samples at $T = 93$ K (tetragonal phase). The second order bands are labelled 1 to 9. R denote the lines linked to the AFD transition. The differences between spectra are pointed by A, B and C.

III. ANALYSIS

1. Generalities on Chemometric analysis and PCA

Generally, chemometric analysis concerns statistical and mathematical methods for extracting information from large numbers of data[20,21]. It is widely used in IR spectroscopy[22] and more and more in Raman studies[23]. Several methods can be used to correlate linearly spectral changes with experimental parameters or to extract each component signal from a mixture. Here is shown

how Principal Components Analysis (PCA) can be efficiently used to extract more information from spectra recorded in STO, which are very complicated and/or display very weak changes. The principle of a PCA is to reduce the number of spectral variables using an orthogonal transformation and turn them into uncorrelated variables called principal components (PC) ranked in order of largest possible variance[24]. Raman spectra have spectral variables which are reduced by PCA to scores and loadings. Scores are the weights of the spectra in the different dimensions (PC) and loadings are the representation of these dimensions according to the wavenumbers. The distribution of these scores in the space of dimensions is used to group or rank individuals (spectra) according to common principal components and thus to link them to a physical parameter. Signal processing, PCA and regression were performed according to a self-made program using the R language and the FactoMineR library[25].

2. Results

As shown above the Raman spectra in STO are rather complex and involve lines with different origins. The PCA is used here to decorrelate in the changes of Raman spectra the pure effect of temperature from the influence of reduction which is here of our interest. The PCA was done on 12 Raman spectra grouping the two sets obtained on untreated and reduced samples, from 100 to 1200 cm^{-1}.

The analysis was done after applying a standard normal variate (SNV) pretreatment on the spectra. The transformation is applied to each spectrum individually by subtracting the spectrum mean and scaling with the spectrum standard deviation, in order to normalize the intensity and to correct the baseline of all spectra.

In Fig. 7 are plotted the scores of the two first components PC1 and PC2 derived from PCA analysis. The scores for each sample can be deduced by projection on axis for both components.

The total variance associated to PC1 and PC2 are equal to 96% so that all the variance in spectra can be nearly explained by both components. A clear separation is obtained between both samples along the axis PC2. The opposite signs reflect the opposite variations in intensities with respect of the mean spectrum between the untreated and reduced crystals. The influence of temperature on the spectra is clearly seen on the PC1 axis for both samples. Indeed, projecting the scores of both samples on the axis PC1 it is shown that the spectra are classified according to T change.

These results provide distinct effects of the two experimental parameters causing changes of the Raman intensities: the sample treatment (on PC2) and the temperature (on PC1). The discrepancy between spectra at the same T is enlarging for lowest T: 133 K and 93 K, indicating a strengthening of the reducing treatment effect on these spectra, consistently with the direct comparison

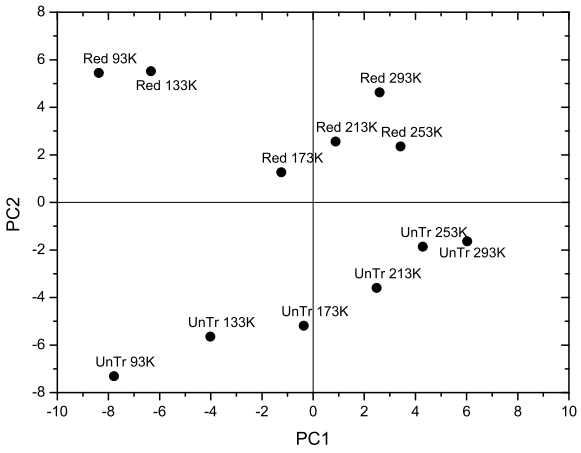

FIG. 7. Scores derived from principal components analysis: PC1 (53% of total variance) and PC2 (43% of total variance) for untreated ($UnTr$) and reduced (Red) samples at each temperature.

of spectra (Figs. 4, 5, 6).

The loadings of the corresponding components are presented in Fig. 8. They represent the value of each component at every point of the spectrum and therefore provide the influence of each component on the spectrum.

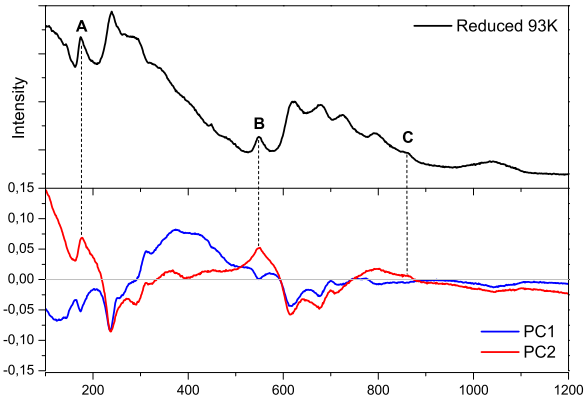

FIG. 8. Principal components analysis : loadings of PC1 and PC2 (lower part) compared to the experimental Raman spectrum of the reduced sample at 93K (upper part).

We observe the variations of Raman intensities vs wavenumber due to the main components. As shown in PC1, the part of the spectrum between 300 and 600 cm^{-1} is very sensitive to T and the intensity increases with T for both samples. In PC2 the positive changes in several wavenumber ranges reflect the difference of Raman spectra between both samples and thus the reduction effect. It is to be underlined that some among these fea-

tures correspond to the peak positions A, B and C of the Raman spectra on the treated sample. We receive confirmation that these peaks are linearly correlated, thus coming from the same physical process induced by the reduction treatment, likely related to oxygen vacancies. Furthermore, PC2 points out below 150 cm^{-1} a positive contribution which could result from V_O as well as the peaks A, B and C.

IV. INTERPRETATION AND DISCUSSION

We have shown above that the Raman spectra on the reduced sample exhibit lines A, B and C, which are attributed to V_O from the direct comparison between untreated and treated samples and PCA applied to all data. Nevertheless our spectra in the reduced crystal are significantly different from those reported by Tenne et al[10]. In particular, in our studies we did not observe the lines (lying around 505, 630, 700 cm^{-1}) attributed by Tenne et al. to local vibrationnal modes associated to V_O. The origin of the discrepancy between previous data and our results is not very clear.

Nevertheless we note that Tenne et al. have performed measurements at much lower temperature (10K). In our studies the lines A, B and C are detected in cubic phase as in the tetragonal phase, in both sides of the AFD transition (110K). The additional lines detected by Tenne et al. do not correspond to cubic stoichiometric STO lattice and, to our opinion, could be due to a process different from this induced by V_O only. Indeed, we can note that their spectra appear relatively close to those reported in Fe- doped STO samples. In these samples, the Raman spectra on the Fe- doped samples exhibit a strong peak around 690- 730 cm^{-1}[26–28], which appears very similar to the highly intense peak attributed by Tenne to be due to V_O. This peak occurs in nanoparticles[27,28] and in single crystals[26] as well. We can therefore assume that the additional lines reported by Tenne et al., is due to local vibrations including both Fe and V_O.

In cubic undoped STO all first-order Raman lines are symmetry forbidden and optical phonons can be obtained by hyper- Raman measurements only. It is remarkable that the lines A, B and C of the reduced sample correspond to the positions if 1^{st} order lines TO_2+LO_1, TO_4 and LO_4 of the pure stoichiometric STO lattice, respectively, as detected by hyper-Raman[29,30].

The new peaks are therefore due to the activation by local symmetry lowering, due to oxygen vacancies, and are assigned to zone center optical phonons of STO lattice. The strong scattering at low frequency (below 150 cm^{-1}) in the reduced sample likely arises from the same phenomenon by the activation of the soft mode TO_1.

According to lattice dynamics calculations[31,32] the TO_2 phonon corresponds to the vibration of Sr ions against TiO_6 octahedra while TO_3 involves Ti-O stretching. Besides the TO_1 ferroelectric soft mode, they are the TO components of the three F_{1u} modes of the cubic phase. No indication of the TO_3 phonon expected at 264 cm^{-1}, corresponding to the silent and non-polar F_{2u} mode is seen in our spectra.

The detection of forbidden 1^{st} order lines was previously reported in nominally pure single crystals[14], thin films[17], ceramics[16] or nanocubes[33]. In fact, grains in ceramics, strain in thin films, or Sr deficiency, likewise O vacancies in our investigation, cause a breakdown of selection rules leading to the detection of 1st order peaks.

An unified explanation can be therefore deduced from these observations, whatever is the nature of the STO material (ceramic, thin film, and single crystal) and its intrinsic point defects related to non-stoichiometry.

The second peculiar feature of the Raman spectra of the reduced $SrTiO_3$ sample is the asymmetric line shape shown by the activated lines A and B. This asymmetry results from the breakdown of the translation symmetry of the crystal, and is thus an additional consequence of the presence of O vacancies. Indeed, in a perfect crystal only optical phonons with a wave vector $q = 0$ (or close to it) can participate to the Raman scattering. The corresponding line is symmetric and centered on the phonon frequency (if its damping or line width is not so large). By contrast, in defected material, O vacancies (in relatively large concentration) or any kind of point defect break the symmetry of the STO lattice, creating locally distorted regions. This induces a relaxation of Raman selection rules, leading to the detection of phonons with a wave vector q which can differ from zero. This gives an asymmetric broadening of the Raman line. Earlier Sirenko et al.[17] have pointed out this asymmetry for the line at 175 cm^{-1} and interpreted it as a Fano resonance. Fano line shapes have been described as the interaction of a phonon and a continuum, arising from rapid polarization fluctuations in polar nano-regions induced by impurities. We invoke here a different interpretation of the line asymmetry, which was at first proposed by Richter et al.[34] in the framework of the phonon confinement model, and which is now more and more used for nano-structures[35,36].

Accordingly, in our model we assume the reduced $SrTiO_3$ compound sample as a sum of spherical regions around each V_O pair with a radius L (the mean size of regions). Assuming that all V_O in the reduced sample are paired, there are 0.25% pairs, each occupying a region of average size $L = 4.6a$ (a is the cell parameter).

We express the 1^{st} induced Raman line shape as a summation of all phonons into the BZ between $q = 0$ and $q_{max} = \pi/L$, supposing an isotropic phonon dispersion:

$$S(\omega) = \int_0^{q_{max}} \frac{C(q)\mathrm{d}q}{((\omega - \omega(q))^2 + (\gamma/2)^2}, \qquad (2)$$

where γ is the linewidth in the stoichiometric material, q is the wave vector in units $2\pi/a$, $\omega(q)$ is the phonon dispersion and $C(q)$, considering a Gaussian distribution, is the weight of each phonon:

$$C(q) = \exp\left(-q^2\pi^2/4\right). \quad (3)$$

The spectral response $S(\omega)$ or line shape of the Raman line therefore depends on the dispersion curve of the phonon $\omega(q)$, and varies with q_{max} and then L. Results of the calculations performed for different values of L (as a multiple of the cell parameter a) are shown in figure 9.

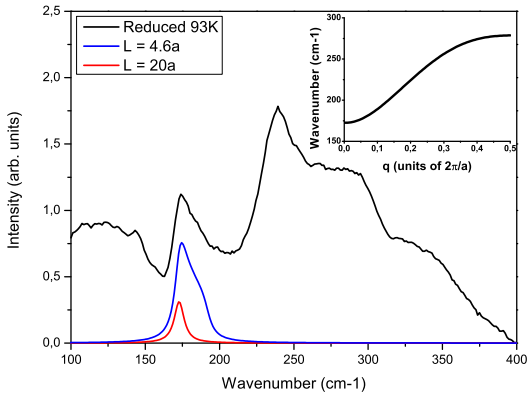

FIG. 9. Raman line shape calculations derived from Eq. 2 with $L = 20a$ (nearly stoichiometric crystal) and then $L = 4.6a$ (crystal with defects) with $\gamma = 8$ cm^{-1} compared to Raman spectrum of the reduced sample at 93 K corrected by the Bose-Einstein thermal population factor. The dispersion branch of the TO_2 phonon[31] used in the calculations is reported in the inset.

We observe that if L is very large (i.e. q_{max} small, case of perfect stoichiometric crystal) the line is symmetric and centered on the frequency ω_0 which corresponds to the frequency at the Brillouin zone center (see the dispersion branch in the insert). By contrast, for small values of L (large concentration of defects), we obtain a broadening of lines, with an asymmetric shape in the high frequency side.

According to this analysis, it can be concluded that no new modes specifically associated with isolated or aggregated V_O appear in the Raman spectra, but the distortions induced by these defects activate scattering from the main transverse optic modes, otherwise forbidden in the cubic lattice. In addition, the broadening of the new peaks is well accounted for by the confinement of phonons within the volumes defined by the defects, if almost all the V_O are assumed to be paired, as indicated by the anelastic spectra.

V. CONCLUSION

The Raman spectra of $SrTiO_3$ can exhibit lines due to different processes: second-order scattering and first-order scattering induced by defects or by the AFD transition. The Principal Component Analysis of data recorded in both as-grown and reduced samples, highlights lines directly related to V_O, whose concentration and aggregation state have been characterized by anelastic relaxation measurements. These bands in fact correspond to the activation of Brillouin zone center optical phonons which are in principle forbidden in stoichiometric material but are related to the breakdown of selection rules caused by the presence of V_O. These peaks, denoted A (phonon TO_2+LO_1) and B (phonon TO_4), are asymmetric in the high frequency side. This asymmetric line shape results from V_O as well, which form distorted regions breaking the translational symmetry, so that phonons out from the Brillouin zone center take part to the scattering. The asymmetric broadening is relatively well reproduced by our model based upon clusters of size inversely proportional to the V_O concentration, assumed to be completely paired below room temperature. Our study underlines the ability of Raman spectroscopy to probe oxygen deficiency, even in a relatively small content. Furthermore, the asymmetric line broadening can be used to estimate the size of distorted regions around V_O.

[1] K. A. Müller and H. Burkard, "Srtio$_3$: An intrinsic quantum paraelectric below 4 k," Phys. Rev. B **19**, 3593–3602 (1979).
[2] S. Gevorgidan, "Ferroelectrics in microwave devices, circuits and systems. physics, modelling, fabrication and measurements," (2009).
[3] C. W. Rischau, X. Lin, C. P. Grams, D. Finck, S. Harms, J. Engelmayer, T. Lorenz, Y. Gallais, B. Fauqué, J. Hemberger, and K. Behnia, "A ferroelectric quantum phase transition inside the superconducting dome of sr1xcaxtio3," Nature Physics **13**, 643 EP – (2017).
[4] Z. Wang, M. Cao, Z. Yao, Q. Zhang, Z. Song, W. Hu, Q. Xu, H. Hao, H. Liu, and Z. Yu, "Giant permittivity and low dielectric loss of srtio3 ceramics sintered in nitrogen atmosphere," Journal of the European Ceramic Society **34**, 1755 – 1760 (2014).
[5] J. S. Lee, S. Lee, and T. W. Noh, "Resistive switching phenomena: A review of statistical physics approaches," Applied Physics Reviews **2**, 031303 (2015), https://doi.org/10.1063/1.4929512.
[6] F. Cordero, "Hopping and clustering of oxygen vacancies in SrTio$_3$ by anelastic relaxation," Phys. Rev. B **76**, 172106 (2007).
[7] A. Hackmann and O. Kanert, "Nmr investigation of defect properties in single crystal srtio3," Radiation Effects and Defects in Solids **119-121**, 651–656 (1991), https://doi.org/10.1080/10420159108220797.
[8] K. Szot, W. Speier, R. Carius, U. Zastrow, and W. Beyer, "Localized metallic conductivity and self-healing during thermal reduction of srtio$_3$," Phys. Rev. Lett. **88**, 075508 (2002).
[9] M. D. Fontana and P. Bourson, "Microstructure and defects probed by raman spectroscopy in lithium niobate crystals and devices," Applied Physics Reviews **2**, 040602 (2015), https://doi.org/10.1063/1.4934203.
[10] D. A. Tenne, I. E. Gonenli, A. Soukiassian, D. G. Schlom, S. M. Nakhmanson, K. M. Rabe, and X. X. Xi, "Raman study of oxygen reduced and re-oxidized strontium titanate," Phys. Rev. B **76**, 024303 (2007).
[11] C. H. Perry, J. H. Fertel, and T. F. McNelly, "Temperature dependence of the raman spectrum of srtio3 and ktao3," The Journal of Chemical Physics **47**, 1619–1625 (1967), https://doi.org/10.1063/1.1712142.
[12] W. G. Nilsen and J. G. Skinner, "Raman spectrum of strontium titanate," The Journal of Chemical Physics **48**, 2240–2248 (1968), https://doi.org/10.1063/1.1669418.

[13]J. Petzelt, T. Ostapchuk, I. Gregora, I. Rychetský, S. Hoffmann-Eifert, A. V. Pronin, Y. Yuzyuk, B. P. Gorshunov, S. Kamba, V. Bovtun, J. Pokorný, M. Savinov, V. Porokhonskyy, D. Rafaja, P. Vaněk, A. Almeida, M. R. Chaves, A. A. Volkov, M. Dressel, and R. Waser, "Dielectric, infrared, and raman response of undoped $srtio_3$ ceramics: Evidence of polar grain boundaries," Phys. Rev. B **64**, 184111 (2001).

[14]H. W. Jang, A. Kumar, S. Denev, M. D. Biegalski, P. Maksymovych, C. W. Bark, C. T. Nelson, C. M. Folkman, S. H. Baek, N. Balke, C. M. Brooks, D. A. Tenne, D. G. Schlom, L. Q. Chen, X. Q. Pan, S. V. Kalinin, V. Gopalan, and C. B. Eom, "Ferroelectricity in strain-free $srtio_3$ thin films," Phys. Rev. Lett. **104**, 197601 (2010).

[15]R. Ouillon, J.-P. Pinan-Lucarre, P. Ranson, P. Pruzan, S. K. Mishra, R. Ranjan, and D. Pandey, "A raman scattering study of the phase transitions in srtio 3 and in the mixed system (sr 1-x ca x)tio 3 at ambient pressure from t = 300 k down to 8 k," Journal of Physics: Condensed Matter **14**, 2079 (2002).

[16]T. Ostapchuk, J. Petzelt, V. Železný, A. Pashkin, J. Pokorný, I. Drbohlav, R. Kužel, D. Rafaja, B. P. Gorshunov, M. Dressel, C. Ohly, S. Hoffmann-Eifert, and R. Waser, "Origin of soft-mode stiffening and reduced dielectric response in $srtio_3$ thin films," Phys. Rev. B **66**, 235406 (2002).

[17]A. A. Sirenko, I. A. Akimov, J. R. Fox, A. M. Clark, H.-C. Li, W. Si, and X. X. Xi, "Observation of the first-order raman scattering in $srtio_3$ thin films," Phys. Rev. Lett. **82**, 4500–4503 (1999).

[18]F. Cordero, L. D. Bella, F. Corvasce, P. M. Latino, and A. Morbidini, "An insert for anelastic spectroscopy measurements from 80 k to 1100 k," Measurement Science and Technology **20**, 015702 (2009).

[19]F. Cordero, "Anelastic (dielectric) relaxation of point defects at any concentration, with blocking effects and formation of complexes," Phys. Rev. B **47**, 7674–7685 (1993).

[20]S. Wold, "Chemometrics; what do we mean with it, and what do we want from it?" Chemometrics and Intelligent Laboratory Systems **30**, 109 – 115 (1995), inCINC '94 Selected papers from the First International Chemometrics Internet Conference.

[21]S. Wold and M. Sjstrm, "Chemometrics, present and future success," Chemometrics and Intelligent Laboratory Systems **44**, 3 – 14 (1998).

[22]C. Muehlethaler, G. Massonnet, and P. Esseiva, "The application of chemometrics on infrared and raman spectra as a tool for the forensic analysis of paints," Forensic Science International **209**, 173 – 182 (2011).

[23]O. Svensson, M. Josefson, and F. W. Langkilde, "Reaction monitoring using raman spectroscopy and chemometrics," Chemometrics and Intelligent Laboratory Systems **49**, 49 – 66 (1999).

[24]H.-C. Kim, D. Kim, and S. Y. Bang, "An efficient model order selection for pca mixture model," Pattern Recognition Letters **24**, 1385 – 1393 (2003).

[25]S. L, J. Josse, and F. Husson, "Factominer: An r package for multivariate analysis," Journal of Statistical Software, Articles **25**, 1–18 (2008).

[26]C. Lenser, A. Kalinko, A. Kuzmin, D. Berzins, J. Purans, K. Szot, R. Waser, and R. Dittmann, "Spectroscopic study of the electric field induced valence change of fe-defect centers in srtio3," Phys. Chem. Chem. Phys. **13**, 20779–20786 (2011).

[27]N. Van Minh and D. T. T. Phuong, "Dopant effects on the structural, low temperature raman scattering and electrical transport properties in srti1xfexo3 nanoparticles synthesized by sol-gel method," Journal of Sol-Gel Science and Technology **55**, 255–260 (2010).

[28]N. Van Minh and D. T. T. Phuong, "Srti1xfexo3 nanoparticle: a study of structural, optical, impedance and magnetic properties," Journal of Experimental Nanoscience **6**, 226–237 (2011), https://doi.org/10.1080/17458080.2010.492841.

[29]H. Vogt, "Hyper-raman tensors of the zone-center optical phonons in $srtio_3$ and $ktao_3$," Phys. Rev. B **38**, 5699–5708 (1988).

[30]Inoue, K. and Asai, N., "Hyper-raman scattering study of ferroelectric phase transitions in srtio3 and batio3," J. Phys. Colloques **42**, C6–430–C6–432 (1981).

[31]W. G. Stirling, "Neutron inelastic scattering study of the lattice dynamics of strontium titanate: harmonic models," Journal of Physics C: Solid State Physics **5**, 2711 (1972).

[32]R. A. Cowley, "Lattice dynamics and phase transitions of strontium titanate," Phys. Rev. **134**, A981–A997 (1964).

[33]S. Banerjee, D.-I. Kim, R. D. Robinson, I. P. Herman, Y. Mao, and S. S. Wong, "Observation of fano asymmetry in raman spectra of srtio3 and caxsr1xtio3 perovskite nanocubes," Applied Physics Letters **89**, 223130 (2006), https://doi.org/10.1063/1.2400095.

[34]H. Richter, Z. Wang, and L. Ley, "The one phonon raman spectrum in microcrystalline silicon," Solid State Communications **39**, 625 – 629 (1981).

[35]K. Adu, Q. Xiong, H. Gutierrez, G. Chen, and P. Eklund, "Raman scattering as a probe of phonon confinement and surface optical modes in semiconducting nanowires," Applied Physics A **85**, 287 (2006).

[36]R. Kumar, G. Sahu, S. K. Saxena, H. M. Rai, and P. R. Sagdeo, "Qualitative evolution of asymmetric raman line-shape for nanostructures," Silicon **6**, 117–121 (2014).